Chinese Journal of
POLYMER SCIENCE

RESEARCH ARTICLE

https://doi.org/10.1007/s10118-023-2958-7
Chinese J. Polym. Sci. **2023**, *41*, 1747–1759

Paclitaxel Prodrug Nanomedicine for Potential CT-imaging Guided Breast Cancer Therapy

Jia-Wei Chen, Yi Shen, Qing-Song Yu*, and Zhi-Hua Gan

State Key Laboratory of Organic-Inorganic Composite Materials, Beijing Laboratory of Biomedical Materials, Beijing Advanced Innovation Center for Soft Matter Science and Engineering, College of Life Science and Technology, Beijing University of Chemical Technology, Beijing 100029, China

Electronic Supplementary Information

Abstract Nanotheranostics, which combine the therapeutic and diagnostic functions in one integrated system, have received extensive attentions in cancer treatments because they enable non-invasive diagnosis, tumor-targeted drug delivery, and real-time monitoring of therapeutic response. However, due to the high systemic toxicity of commonly used chemotherapeutics, current treatment still has limitations. Herein, to simultaneously achieve safe cancer therapy and therapeutic response monitoring, an iodinated prodrug strategy was proposed. 2,3,5-Triiodobenzoic acid (TIBA) was used to modify both paclitaxel (PTX) and the polymeric vehicle, so that the encapsulation efficiency of PTX could be increased and the systemic toxicity could be reduced. As-prepared prodrug nanoparticles could accumulate passively in the tumor site and promptly release loaded drugs in response to the overexpressed GSH in cancer cells, which then caused efficient cell cycle arrest and apoptosis like that of the parent PTX. With this rational design, safe and efficient antitumor therapy and real-time computer tomography (CT) imaging could be simultaneously realized, facilitating potential CT imaging-guided therapy of metastatic breast cancer.

Keywords CT imaging; Paclitaxel; Prodrug; GSH responsiveness; Polymeric nanoparticles

Citation: Chen, J. W.; Shen, Y.; Yu, Q. S.; Gan, Z. H. Paclitaxel prodrug nanomedicine for potential CT-imaging guided breast cancer therapy. *Chinese J. Polym. Sci.* **2023**, *41*, 1747–1759.

INTRODUCTION

Cancer nanotheranostics, which combine the therapeutic and diagnostic functions in one integrated system, have received extensive attentions because they enable the non-invasive diagnosis, tumor targeted drug delivery and real-time monitoring of therapeutic response.[1–4] Computed tomography (CT) imaging, which uses high-atomic number elements (such as iodine, platinum and gold) as the contrast agents,[5,6] has been widely used in the diagnosis of multiple cancers because of its wide availability, high spatial resolution, unlimited depth, and accurate anatomical information.[7–9] However, the conventional iodinated contrast agents (*e.g.*, Omnipaque) have shown some drawbacks, such as narrow imaging window, renal toxicity, and lack of specificity.[10,11] In contrast, nanosized contrast agents could better serve as theranostics due to their advantages like prolonged circulation time and site-specific accumulation.[12,13]

To simultaneously achieve CT imaging and drug delivery, lots of nanosized CT contrast agents such as iodinated nanoassembly, self-assembly structures of gold nanoparticles have been developed.[14,15] These systems could not only monitor the *in vivo* drug transportation in real time mode, but also diagnose the potential metastasis during treatment.[16,17] Many chemotherapeutic drugs have been incorporated with these nanocarriers to achieve efficient tumor growth inhibition, including paclitaxel (PTX),[18] doxorubicin (DOX),[19] cisplatin,[20] *etc*. However, even though current CT-guided theranostics have greatly altered the pharmacokinetics of loaded drugs and facilitated the treatment and diagnosis of tumor, the involvement of toxic chemotherapeutics in these systems still hindered their safe application.[21] Therefore, it is in urgent need to develop new theranostics that can overcome the dose-limiting toxicity of current ones.

As a widely used chemotherapeutics effective for many solid tumors,[22,23] PTX is the first line dug for metastatic breast cancer.[24] However, due to its intrinsic hydrophobicity and crystallinity, the *in vivo* delivery of PTX remains problematic.[25,26] Fortunately, recent advancements of prodrug nanotechnologies have paved the way for *in vivo* application of PTX. Compared with parent PTX, prodrug strategies significantly altered its physical and chemical properties, facilitating the efficient drug loading and cancer cells selective drug activation.[27,28] Therefore, better safety profiles and cancer selectivity could be achieved with this strategy. Various polymeric or small molecular PTX prodrugs have been developed for either mono- or combinatory therapy.[29–33] These prodrugs could be administered alone or in combination with targeted nanocarrier.[34] Moreover, multiple prodrug could also

* Corresponding author, E-mail: yuqs@mail.buct.edu.cn
Received December 31, 2022; Accepted February 8, 2023; Published online March 23, 2023

be accurately delivered with single engineered nanoplatform to achieve personalized combinatory therapy.[35] However, very few of the reported prodrug nanomedicines could fulfill the need of CT imaging.

Herein, to simultaneously realize efficient PTX delivery and CT imaging, a prodrug strategy based on PTX and iodinated components was proposed. 2,3,5-Triiodobenzoic acid (TIBA) was introduced to synthesize the PTX prodrug and the corresponding delivery vehicle (Scheme 1). Moreover, a disulfide linkage was applied to achieve efficient intracellular drug delivery and deplete the abundant intracellular glutathione, so that potential drug resistance could be avoided.[36–38] A stable nanoparticular drug delivery system was established by coprecipitation of PTX prodrug and vehicle polymer. Therefore, as-prepared redox-sensitive prodrug nanomedicine may provide a new strategy for the safe and efficient delivery of PTX and facilitate the real-time of the therapeutic effect at the same time.

MATERIALS AND METHODS

Materials

Bis(2-hydroxypropyl) disulfide was purchased from Aladdin chemical, Inc. (Shanghai, China). Methoxy poly(ethylene glycol) (M_w=5000, $mPEG_{5k}$), 4,4′-azodi(4-cyanovalerate) (V501), 2,3,5-triiodobenzoic acid (TIBA), 4-*tert*-butylcatechol, 1-(3-dimethylaminopropyl)-3-ethylcarbodiimide hydrochloride (EDC•HCl), *N*,*N*-diisopropylethylamine (DIPEA), hydroxyethyl methacrylate (HEMA), anhydrous dimethyl sulfoxide (DMSO) and Tween 80 were obtained from J&K Chemicals (Beijing, China). Dicyclohexyl carbodiimide (DCC) and 4-dimethylaminopyridine (DMAP) were obtained from Adamas Co., Ltd., (Shanghai, China). Paclitaxel (PTX) was purchased from Huafeng Info United Co., Ltd., (Beijing, China). Nile red, 4′,6-diamidino-2-phenylindole (DAPI) and 3-(4,5-dimethylthiazol-2-yl)-2,5-diphenyltetrazolium bromide (MTT) were purchased from Beyotime Biotechnology Co., Ltd., (Nantong, China). LysoTracker Green DND-26 was purchased from Invitrogen (Beijing local agent, China). PI/Annexin V-FITC apoptosis detection kit and cell cycle analysis kit were purchased from Solarbio Life Sciences Co., Ltd., (Beijing, China). All other chemicals were of reagent grade and used without further purification.

Characterization

^{1}H-NMR spectrum was performed on a Bruker AVANCE III 400 MHz NMR spectrometer (Bruker, Germany) with $CDCl_3$ and DMSO-d_6. The morphology of nanoparticles was characterized with a transmission electron microscope (TEM, HT-7700; accelerating voltage 120 kV, Hitachi, Ltd., Japan). The size distribution and zeta potential of the nanoparticles were characterized by dynamic light scattering (DLS) using a Zetasizer Nano ZS90 (Malvern Instruments, Malvern, UK) with 90° optics and a He-Ne Laser (4.0 mW, 633 nm). The molecular weights of all polymers were analyzed by gel permeation chromatography (GPC, Waters 1515 GPC setup equipped with a Waters 1515 differential refractive index detector) at 40 °C in 1.0 mL/min of *N*,*N*-dimethylformamide (DMF) containing 20 mmol/L lithium bromide. High performance liquid chromatography (HPLC) traces were recorded by a Shimadzu LC-20 HPLC system (Japan). Flow cytometric (FCM) measurements were performed on a Beckman Coulter CytoFLEX Flow Cytometer (USA). The fluorescent images were captured on a Leica TCS SP8 confocal

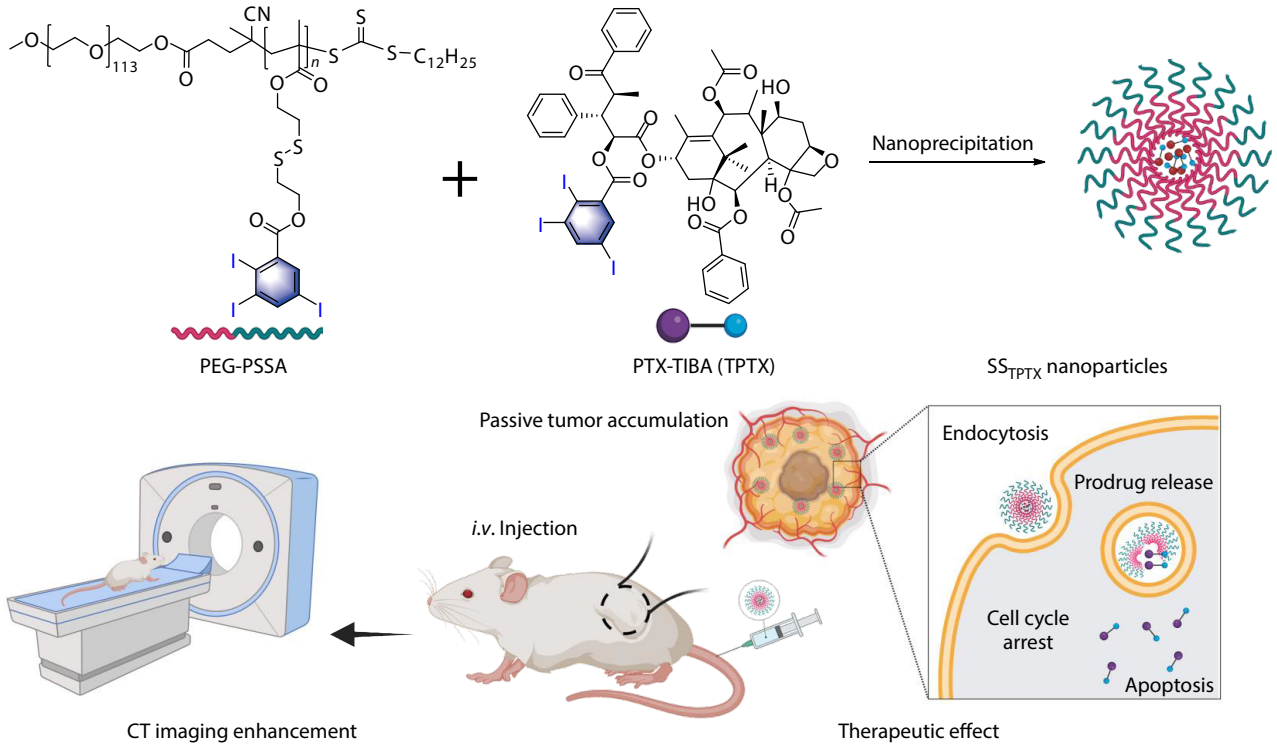

Scheme 1 Fabrication of prodrug nanoparticles and the mechanism of action of the nanoparticles *in vivo* (The illustration was created by Biorender.com).

https://doi.org/10.1007/s10118-023-2958-7

laser scanning microscope (CLSM, Germany). CT images were captured on a Quantum GX small animal microCT apparatus (Perkin Elmer, USA).

Synthesis of PTX-TIBA Prodrug (TPTX)

PTX (0.49 g, 0.57 mmol), TIBA (0.29 g, 0.58 mmol), DCC (0.177 g, 0.86 mmol) and DMAP (0.007 g, 0.06 mmol) were added into 100 mL dry flask, and then anhydrous DMF was added as the solvent. After stirring for 2 days, the byproduct *N*,*N*′-dicyclohexylurea (DCU) was removed by filtration. DMF was then removed by rotary evaporation, and dichloromethane (DCM) was added to dissolve the mixture. The crude product was purified by silica gel chromatography with pure DCM as the mobile phase. The physical and chemical properties of TPTX were characterized by ^{1}H-NMR and X-ray diffraction (XRD).

Synthesis of Polymeric Vehicle Containing Disulfide Bonds (PEG-PSSA)

Synthesis of MA-SS-OH monomer

Bis(2-hydroxypropyl) disulfide (10 mL, 75.98 mmol) and triethylamine (5 mL, 35.97 mmol) were dissolved in 60 mL of ethyl acetate, then methacryloyl chloride (7.4 mL, 76.17 mmol) was added dropwise to the mixture with 4-*tert*-butyl-catechol as the stabilizer. The reaction was maintained in an ice bath overnight and then triethylamine hydrochloride was removed by filtration. Ethyl acetate was replaced with DCM, and the crude product was purified by silica gel chromatography with ethyl acetate/*n*-hexane (1/3, *V*/*V*) as the mobile phase. The chemical structure was characterized by ^{1}H-NMR.

Synthesis of MA-SS-TIBA

MA-SS-OH (1.4 g, 6.30 mmol), TIBA (3.2 g, 6.40 mmol), DCC (1.88 g, 9.11 mmol), and DMAP (0.078 g, 0.64 mmol) were dissolved in 50 mL of anhydrous DMF, and the reaction was maintained at room temperature for 48 h in a dark environment. After removing DCU, the filtrate was concentrated and purified by silica gel column chromatography with DCM as the eluent. The chemical structure of the product was confirmed by ^{1}H-NMR.

Synthesis of PEG-PSSA

MA-SS-TIBA (0.4 g, 0.56 mmol), PEG_{5k}-CTA (2.85 g, 0.56 mmol), V501 (1.4 mg), and DMF (0.7 mL) were added into a Schlenk tube. After three freeze-vacuum-thaw cycles, the polymerization was carried out for 24 h under argon atmosphere. After the reaction, the product was precipitated with cold ethyl acetate, and centrifuged to collect the precipitated products. The molecular weight and chemical structure of the polymer were characterized with GPC and ^{1}H-NMR, respectively.

Synthesis of Polymeric Vehicle without Disulfide Bond (PEG-PA)

Synthesis of HEMA-TIBA

HEMA (2 mL, 16.49 mmol), TIBA (8.24 g, 16.49 mmol), DCC (5.13 g, 24.86 mmol), DMAP (0.2 g, 1.64 mmol), and 50 mL of anhydrous DMF were added in a 100 mL round bottom flask. The reaction was maintained at room temperature for 48 h in a dark place. After removing DCU, the crude product was purified by silica gel using DCM as the eluent. The chemical structure of the product was characterized by ^{1}H-NMR.

Synthesis of PEG-PA

HEMA-TIBA (0.26 g, 0.42 mmol), PEG_{5k}-CTA (2.1 g, 0.41 mmol), V501 (2.8 mg), and 0.9 mL of DMF were added in a Schlenk tube. After three freeze-vacuum-thaw cycles, the polymerization was carried out at 70 °C under argon atmosphere for 24 h. After the reaction, the product was precipitated, centrifuged and collected. The molecular weight and chemical structure of the polymer were characterized by GPC and ^{1}H-NMR, respectively.

Preparation of Empty and Drug-loaded Nnanoparticles

Preparation of drug-loaded nanoparticles

Polymer (10 mg) was mixed with 0.5, 1, 2.5 and 5 mg of TPTX, respectively, and then dissolved in 1 mL of DMF. The mixture was injected into 7 mL of deionized water with a syringe pump with a rate of 1 mL/20min under vigorous stirring. After further stirring for 2 h, the solution was dialyzed against 3500 Da dialysis bag in deionized water to obtain the drug-loaded nanoparticles. At the same time, PTX, Nile red, and Cy7.5 loaded nanoparticles were also fabricated using the same method.

Preparation of empty nanoparticles

Polymer (10 mg) in 1 mL of DMF was injected into 7 mL of deionized water with a syringe pump at a rate of 1 mL/20min. After 2 h stirring, the mixture was dialyzed with a 3500 Da dialysis bag in deionized water to obtain the empty nanoparticles.

Drug Loading Capacity of PEG-PA and PEG-PSSA Polymer

20 mL of 1 mg/mL drug loaded nanoparticles were freeze dried under vacuum. Dry powder (10 mg) was dissolved in 1 mL of anhydrous methanol, and then passed through a 450 nm filter membrane. Finally, the drug content was determined by HPLC. The drug concentration was calculated according to the standard curves of PTX and TPTX, respectively. The drug loading content (DLC%) and drug loading efficiency (DLE%) were calculated according to the following equations:

$$\mathrm{DLC\%} = m_{\mathrm{drug}}/(m_{\mathrm{drug}} + m_{\mathrm{vehicle}}) \times 100\% \quad (1)$$

$$\mathrm{DLE\%} = m_{\mathrm{drug}}/m_{\mathrm{added\ drug}} \times 100\% \quad (2)$$

where m_{drug} is the mass of drugs inside nanoparticle, m_{vehicle} is the mass of vehicle, $m_{\mathrm{added\ drug}}$ is the mass of added drugs.

In vitro Release of TPTX from Drug Loaded Nanoparticles

3 mL of 1 mg/mL drug-loaded nanoparticles was loaded into the 7000 Da dialysis bag. Drug release experiments were carried out at 37 °C in a pH 7.4 buffer solution containing different components (100 μmol/L or 10 mmol/L GSH). 1% Tween 80 was added to the buffer solution to simulate the leak conditions. At predetermined time points (*i.e.*, 0.5, 1, 3, 6, 21, 34, 48, 72 h), 1 mL of dialysate was taken out and replaced with 1 mL of fresh buffer solution. The cumulative drug release was calculated according to the following equation:

$$\text{Cumulative drug release} = C_x \times V + \sum_{k=1}^{k-1} C_k \times v \quad (3)$$

where the PTX concentration measured in x h is recorded as C_x, C_k is any PTX concentration measured before time point k, V is the total volume of the dialysate and v is the sampling volume.

Cytotoxicity Study of Drug Loaded Nanoparticles on 4T1 Cells

4T1 cells were seeded in a 96-well plate (5×10^3 cells/well) at 24 h before the experiments. The culture medium was removed and replenished with 100 μL of fresh medium supplemented with

https://doi.org/10.1007/s10118-023-2958-7

various concentration of drugs. The cells were then cultured at 37 °C for 24 h. After replacement with 100 μL of fresh medium, 10 μL of MTT solution (5 mg/mL) was added to incubate for another 4 h. The MTT-formazan generated by live cells was dissolved by 150 μL of DMSO, and the absorbance at a wavelength of 490 nm of each well was measured using a microplate reader (Multiscan GO, Thermo Scientific).

In vitro Cellular Uptake and Lysosome Colocalization

In vitro cellular uptake

The 4T1 cells were cultured on glass bottom petri dish (5×10^5 cells/well) using DMEM medium at 24 h before the experiments. The cells were incubated with Nile Red labeled PEG-PSSA/TPTX(SS_{TPTX}) and PEG-PA/TPTX(CC_{TPTX}) nanoparticles (PTX dosage: 10 μmol/L) at 37 °C for 1, 3 and 6 h, repectively. After removing the culture medium, the cells were washed with PBS for three times, fixed with 4% paraformaldehyde solution for 15 min and stained with 4,6-diamidino-2-phenylindole (DAPI) for 10 min and finally mounted with glycerol. The fluorescence images were obtained using a CLSM.

Lysosome colocalization

4T1 cells were cultured on glass bottom petri dish (5×10^5 cells/well) using DMEM medium at 24 h before the experiments. The cells were incubated with Nile Red labeled SS_{TPTX} and CC_{TPTX} nanoparticles (PTX dosage: 10 μmol/L) at 37 °C for 6 h. After removing the culture medium, the cells were washed with PBS for three times. The LysoTracker DND-26 (Green) working solution was diluted to an appropriate concentration with culture medium and added to the petri dish to incubate for 30 min. After washing with PBS, the fluorescence images were obtained using a CLSM.

Cell Apoptosis and Cell Cycle Analysis

For the apoptosis study, 4T1 cells in the logarithmic growth phase were seeded in a 6-well plate at a density of 1.5×10^5 cells per well. After incubating for 24 h, cells were treated with PEG-PA, PEG-PSSA, PTX, TPTX, CC_{TPTX} or SS_{TPTX} (PTX dosage: 10 μmol/L) for 12 h at 37 °C. All cells were harvested, suspended in a binding buffer, stained with fluorescein isothiocyanate (FITC)-labeled annexin V (annexin V-FITC) and propidium iodide (PI) for 20 min in the dark, and analyzed by FCM.

For the cell cycle study, 4T1 cells were seeded in a 6-well plate at a density of 1.5×10^5 cells per well. After incubating for 24 h, cells were treated with PEG-PA, PEG-PSSA, PTX, TPTX, CC_{TPTX} or SS_{TPTX} (PTX dosage: 10 μmol/L) for 12 h at 37 °C. Subsequently, cells in each group were harvested, fixed with 70% ethanol at −4 °C overnight. The treated cells were washed by PBS, incubated with RNase, followed by PI (0.1 mg/mL) staining. Cell cycle distribution was analyzed using FCM.

Animal Experiments

BALB/c mice (female, 6 weeks old) were purchased from Beijing HFK Bioscience (Beijing, China). All animals received care in compliance with the guidelines outlined in the Guide for the Care and Use of Laboratory Animals and all procedures were approved by the China-Japan Friendship Hospital Ethics Committee (180209).

In vivo Fluorescent Imaging and CT Imaging of Drug Loaded Nanoparticles

In vivo fluorescent imaging

Each mouse was subcutaneously injected with 100 μL of serum-free medium containing 3.0×10^6 4T1 cells. The mice were randomly divided into three groups after 1 week of feeding until the tumor volume was about 120 mm^3. The drug-loaded nanoparticles containing Cy7.5 (Cy7.5 equivalent, 1 mg/kg) were injected through tail vein. After injection, the mice were anesthetized with isoflurane, and the fluorescence distribution of mice was photographed under λ_{ex}=745 nm and λ_{em}=800 nm using a small animal imaging system (IVIS spectrum, Perkin Elmer) at 1, 3, 6, 12 and 24 h, respectively. After taking 24 h live photos, the mice were sacrificed under anesthesia, the heart, liver, spleen, lung, kidney, and tumor were excised and photographed.

In vivo CT imaging

The iodinated polymer was dissolved in 1 mL of DMF, and injected into 9 mL of water to fabricate 5 mg/mL nanoparticle solution. The nanoparticle was lyophilized using PEG_{2k} as freeze-drying protective additive. Before injection, the nanoparticles were dissolved by water, glucose was used to regulate osmotic pressure. At the same time, iohexol solution containing 50 mg/mL iodine was also prepared as control. The CT imaging was then carried out on a small animal microCT apparatus.

In vivo Antitumor Therapy

To evaluate the *in vivo* antitumor effect of prodrug nanomedicine, subcutaneous 4T1 tumor xenograft was established. When the tumor volume of mice reached 100 mm^3, the mice were randomly divided into 5 groups, and *i.v.* injected with PBS, PTX, TPTX, CC_{TPTX}, and SS_{TPTX}, respectively. The tumor volumes and body weight of mice were examined every 2 days. At the end of the experiments, the tumors were dissected and stained with hematoxylin-eosin staining (H&E), TdT-mediated dUTP nick end labeling (TUNEL) and ki67 to evaluate the antitumor effect. Besides, major organs were also collected and subjected to H&E staining.

Statistical Analysis

All data were reported as averages plus/minus the standard deviation (mean±SD) of at least 3 independent experiments, unless otherwise noted. Statistical significance was assessed by one-way ANOVA with Bonferroni post-tests using GraphPad Prism 8.0 software and $p<0.05$ was considered statistically significant.

RESULTS AND DISCUSSION

Synthesis and Characterization of TPTX, PEG-PA, PEG-PSSA

As a well-known irreversible tubulin stabilizer, PTX can prevent the depolymerization of tubulin and inhibit cell mitosis and proliferation.[39] Considering that the physical and toxicological properties of PTX which lead to low encapsulation efficiency and severe side effects, the prodrug strategy was adopted to improve the loading efficiency and safety profiles. Meanwhile, nanotechnology was utilized to enhance the tumor-specific delivery of as-prepared prodrugs and to improve the ultimate therapeutic efficacy (Scheme 1). The 2′-hydroxyl group of PTX was esterified with TIBA under the reaction conditions as shown in Fig. 1(a). To confirm the successful synthesis of TPTX, the chemical structures of PTX and TPTX were investigated by ^{1}H-NMR (Figs. 1b and 1c). As shown in Fig. 1(b), the appearance of characteristic peaks at 8.31 and 7.74 ppm in the ^{1}H-NMR

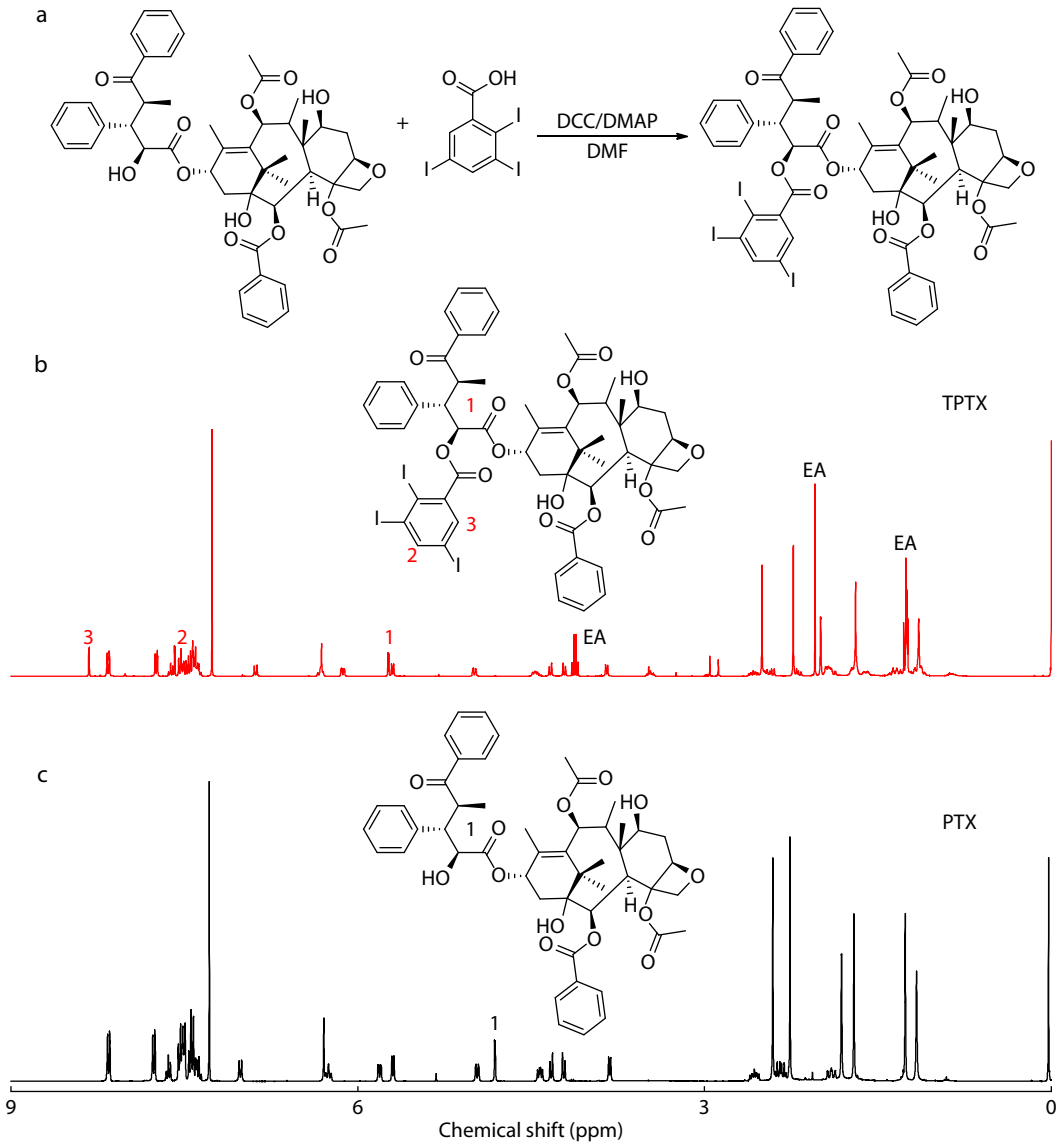

Fig. 1 (a) Synthetic route to TPTX; (b) ^{1}H-NMR sprctrum of TPTX; (c) ^{1}H-NMR spectrum of PTX.

spectrum of TPTX indicated the presence of TIBA residue in the prodrug. Moreover, the chemical shift of 2′-position proton that changed from 4.81 ppm to 5.73 ppm suggested the formation of ester bond with stronger electron-withdrawing ability. Collectively, these results clearly indicated the successful synthesis of TPTX prodrug. In addition, the XRD characterization (Fig. S1 in the electronic supplementary information, ESI) of the resultant TPTX indicated that the 2′-hydroxyl group modification efficiently inhibited the crystalline behavior of PTX, as indicated by the disappearance of the crystalline peak of PTX at 2θ of 15.5°–20.4°, facilitating the subsequent drug encapsulation.

To achieve efficient drug loading and strengthen the CT imaging capacity of as-prepared prodrug, the iodinated polymeric vehicles based on TIBA were also synthesized. The reductive intracellular environment in cancer cells was utilized to facilitate the release of as-designed prodrug.[33] Firstly, one of the hydroxyl groups of dihydroxyl ethyl disulfide was modified with methacryloyl chloride to obtain MA-SS-OH (Fig. S2 in ESI). Then, the rest hydroxyl group of MA-SS-OH was reacted with TIBA to yield the final MA-SS-TIBA monomer. Meanwhile, a GSH insensitive monomer HEMA-TIBA was also synthesized by the esterification between HEMA and TIBA. The chemical structures of MA-SS-TIBA and HEMA-TIBA could be found in Figs. S3 and S4 (in ESI). Based on these monomers, both the GSH-sensitive (PEG-PSSA) (Fig. 2a) and -insensitive (PEG-PA) (Fig. 2c) block polymers were further prepared by reversible addition-fragmentation chain transfer radical polymerization using trithiocarbonate modified PEG (PEG-DDMAT) as the macromolecular chain transfer agent.[40] The structures and molecular weight of the resultant polymers could be confirmed by ^{1}H-NMR (Figs. 2b and 2d) and GPC (Fig. 2e). By comparing the integration ratio of peak a from PEG and peak e from TIBA, the molecular weight of PA and PSSA block was calculated to be 4.5k and 5.3k, respectively. Meanwhile, relatively narrow molecular weight distribution (PDI≤1.20) was observed from the GPC elution curves of both polymers, indicating their well-defined structures.

https://doi.org/10.1007/s10118-023-2958-7

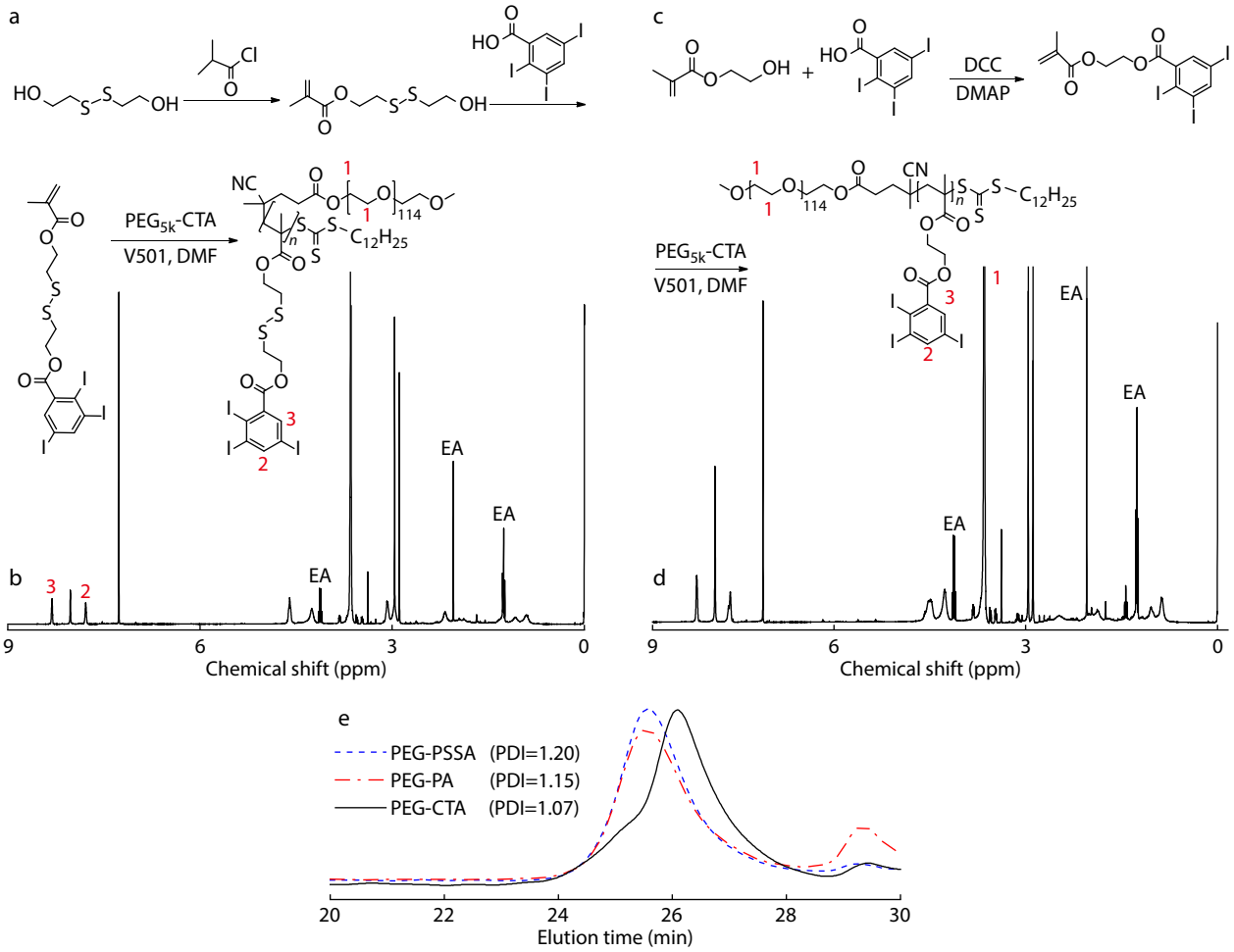

Fig. 2 (a) Synthetic route of PEG-PSSA; (b) ^{1}H-NMR of PEG-PSSA; (c) Synthetic route of PEG-PA; (d) ^{1}H-NMR of PEG-PA; (e) GPC curves of PEG-PSSA, PEG-PA, PEG-CTA.

Characterization of Prodrug Nanoparticles

To increase the water solubility of TPTX prodrug and achieve the efficient *in vivo* delivery, prodrug nanoparticles based on TPTX and PEG-PA/PEG-PSSA were fabricated using simple nanoprecipitation method. The DLC of PTX and TPTX at various polymer/drug ratios were tested. As shown in Table S1 (in ESI), in a wide polymer/drug ratio range from 10/0.5 to 10/5, TPTX could be efficiently loaded by both PEG-PA and PEG-PSSA, with similar actual DLC and theoretical DLC observed in various polymer/drug ratios. In contrast, there is a large deviation between the theoretical DLC and the actual DLC for PTX loaded by PEG-PA polymer. The significantly enhanced drug encapsulation efficiency of TPTX prodrug might be attributed to the chemical modification of 2′-OH, which increased the hydrophobicity and decreased the crystallinity of PTX. After balancing the CT imaging capability with potential toxicity, nanoparticles with DLC of 10% were used in the subsequent experiments.

The hydrodynamic properties of as-prepared nanoparticles were characterized by DLS. As shown in Fig. 3(a), the sizes of the PEG-PA, CC_{TPTX}, PEG-PSSA and SS_{TPTX} nanoparticles are 39.1±1.5, 81.2±1.1, 56.2±1.3, 102.7±1.5 nm, respectively. The larger size of drug loaded nanoparticles than drug-free nanoparticles could be attributed to the loaded TPTX. And the narrow size distribution of the CC_{TPTX} and SS_{TPTX} nanoparticles (PDI<0.2) could be attributed to the well-defined structure of the polymer and the strong interaction between the polymers and prodrugs. This could be further confirmed by the TEM results (Fig. 3c), which showed the spherical morphology of the nanoparticles. The zeta potentials of these nanoparticles are −9.5±0.4, −12.9±0.5, −9.8±0.5 and −14.9±0.3 mV, respectively (Fig. 3b). The negatively charged surface may better protect loaded drugs and avoid nonspecific accumulation in monophagocytic systems.[41]

Notably, due to the strong *π*-*π* interaction between prodrugs and polymers, superior stability could be obtained for as-prepared nanoparticles in 10% FBS DMEM (Fig. 3d), ensuring the stable *in vivo* transportation. It has been reported that the content of intracellular GSH of cancer cells was about 1000 times of the extracellular GSH, the GSH-responsiveness may significantly facilitate the intracellular drug release.[42] The release profiles of TPTX from GSH-sensitive or -insensitive nanoparticles were further investigated using HPLC. The results revealed that approximately 25% TPTX was released from both SS_{TPTX} and CC_{TPTX} in 72 h under physiological conditions in the absence of 100 μmol/L or 10 mmol/L GSH (Fig. 3e). In contrast, compared with the insignificant increase of TPTX release from CC_{TPTX}, more than 90% of loaded TPTX was re-

https://doi.org/10.1007/s10118-023-2958-7

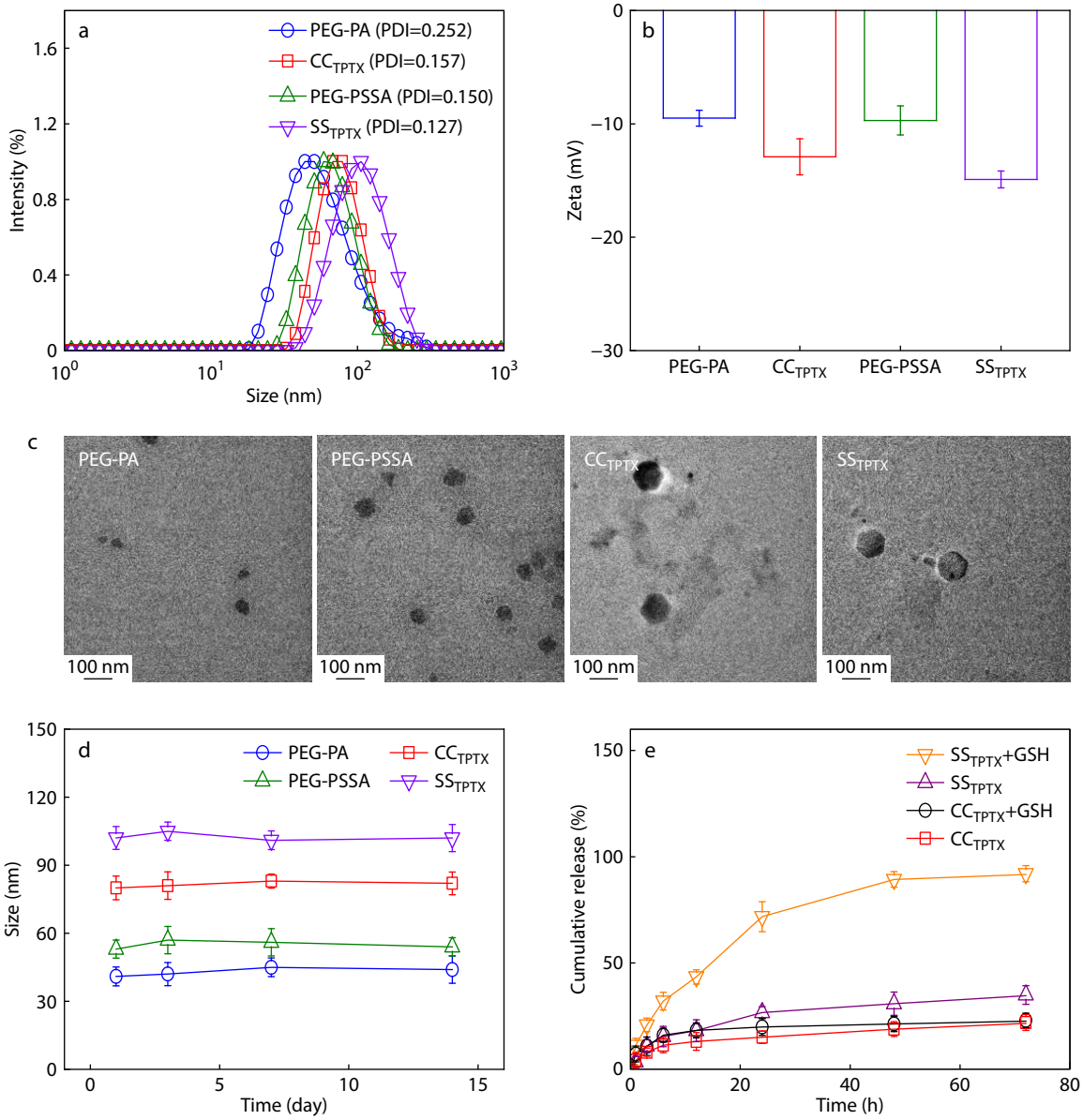

Fig. 3 (a) Size distribution of PEG-PA, PEG-PSSA, CC$_{TPTX}$ and SS$_{TPTX}$; (b) Zeta potential of PEG-PA, PEG-PSSA, CC$_{TPTX}$, and SS$_{TPTX}$; (c) TEM images of PEG-PA, PEG-PSSA, CC$_{TPTX}$ and SS$_{TPTX}$; (d) The stability of PEG-PA, PEG-PSSA, CC$_{TPTX}$ and SS$_{TPTX}$ in DMEM medium containing 10% FBS; (e) *In vitro* drug release profiles of drug-loaded micelles under various environments (with 100 μmol/L or 10 mmol/L GSH). Data are presented as mean±SD (n=3, **p<0.01, ***p<0.001).

leased from SS$_{TPTX}$ in 72 h in the presence of 100 μmol/L or 10 mmol/L GSH, possibly due to the rapid disassembly of the nanoparticles under reductive environment. The rapid drug release under the simulated intracellular reductive condition suggested that the prodrug might be efficiently released from the nanoparticles inside cells to avoid the acquired drug resistance derived from low concentration drug stimulation.[43]

Cellular Uptake and Lysosomal Colocalization

The efficient cellular uptake and rapid intracellular drug release is the prerequisite for the therapeutic effect of nanomedicine.[44] To investigate the cellular uptake and intracellular drug delivery, Nile Red-labeled CC$_{TPTX}$ and SS$_{TPTX}$ nanoparticles were co-incubated with 4T1 cells. The Nile red fluorescence at different time after adding nanoparticles were observed by the CLSM (Fig. 4a). CLSM images show that the intracellular fluorescence significantly increased with increasing time in both groups. Moreover, the intracellular fluorescence of the SS$_{TPTX}$ group was higher than that of the CC$_{TPTX}$ group. This could be further confirmed by the quantitative analysis of intracellular Nile red content (Fig. 4b), in which SS$_{TPTX}$ groups showed higher intracellular dye content than the insensitive group. The higher cellular uptake of the GSH-sensitive nanoparticle could be explained by its larger size, which facilitated endocytosis by cancer cells.[45]

After being ingested by cells, most nanoparticles are disintegrated in lysosomes to release the loaded drugs.[46] To monitor the intracellular drug release of nanoparticles in cancer

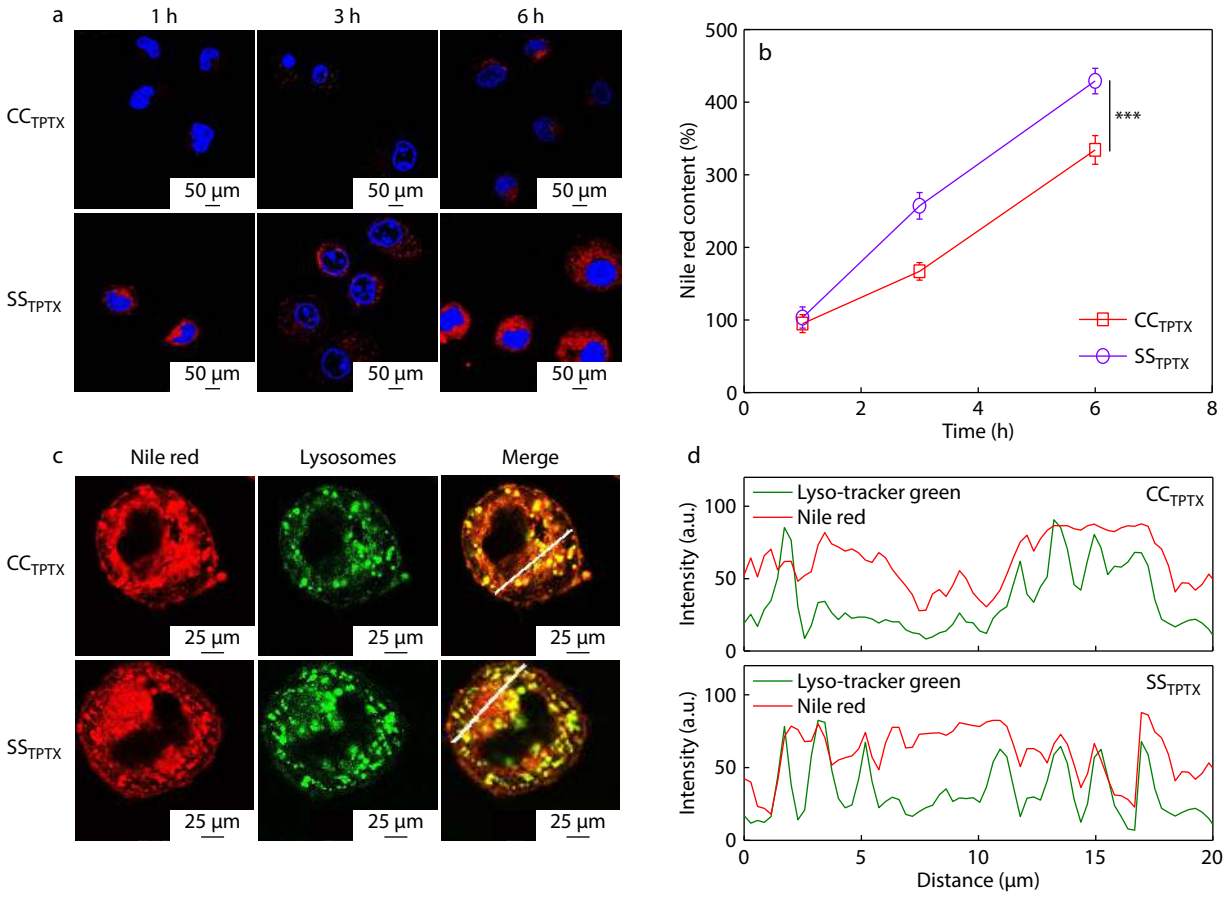

Fig. 4 (a) CLSM images of 4T1 cells at 1, 3 and 6 h after incubation with different Nile red labeled prodrug nanoparticles (red). Cell nucleus was stained with DAPI (blue). Scale bar=50 μm. (b) Quantitative analyses of Nile Red content in cancer cells; (c) CLSM images of 4T1 cells following incubation with Nile red labeled CC_{TPTX} or SS_{TPTX} for 6 h. Lysosomes were stained with LysoTracker DND-26 (green). Scale bar=25 μm. (d) Line profile analyses of Nile red and lysosome colocalization in cancer cells. Data are presented as mean±SD (n=3, $^{**}p$<0.01, $^{***}p$<0.001).

cells, the subcellular colocalization between Nile red labeled nanoparticles (red) and lysosomes (green). As shown in Fig. 4(c), the Nile red fluorescence of CC_{TPTX} nanoparticles fully colocalized with lysosomes, suggesting that lysosomal pathway was involved in the intracellular transportation of the nanoparticles. In contrast, the Nile red fluorescence of SS_{TPTX} was partially colocalized with lysosomes, indicating the drug release from the nanoparticles. These results could be further confirmed by the line profile analyses (Fig. 4d), in which the partial colocalization of SS_{TPTX} with lysosomes was clearly presented. These results indicated that as-prepared GSH-sensitive nanoparticles could be efficiently endocytosed by cancer cells to release the loaded drugs in response to the intracellular GSH.

Apoptosis, Cell Cycle Arrest and Cytotoxicity Caused by the Prodrug Nanoparticles

One of the key features of prodrug nanomedicine is the selective activation in cancer cells which simultaneously maintain the activity of parent drug and improve the safety profiles.[47] To evaluate whether the chemical modification altered the therapeutic effect of the parent PTX, the cell cycle analysis, apoptosis assay, and cytotoxicity assay was carried out with 4T1 cells. The typical feature of PTX is the G2/M phase arrest which caused the apoptosis of cancer cells and sensitize the treated cells to other treatments.[48] Therefore, we first characterized the cell cycle distribution of 4T1 cells treated with various drugs (Figs. 5a and 5c). Compared with PBS group, both PEG-PA and PEG-PSSA treatments cause no obvious cell cycle arrest. The PTX treatment could significantly increase the G2/M population from 3.47% to 71.2%. Similarly, a G2/M population of 67.3% could be obtained after the treatment with TPTX prodrug, suggesting that the chemical modification did not change the mechanism of action of PTX inside cancer cells. After loading by PEG-PA (CC_{TPTX}) and PEG-PSSA (SS_{TPTX}), the G2/M population decreases to 35.9% and 49.8%, respectively, possibly due to their different endocytosis mechanism from free drugs. The higher G2/M population of GSH-sensitive nanoparticles than insensitive nanoparticles could be attributed to the rapider intracellular drug release.

The apoptotic rate of 4T1 cells treated with various drugs was characterized by the double staining with Annexin V-FITC and PI (Figs. 5b and 5d). PTX and TPTX caused a similar apoptotic proportion of 46.5%, located mainly in the late apoptosis quadrant. Slightly lower number of apoptotic cells could be found for SS_{TPTX} (36.5%) and CC_{TPTX} (35.9%) treatments, in accordance with their cell cycle arrest. To further explore the dose dependent toxicity of various drugs on 4T1 cells, the survival rate of tumor cells after various treatments was meas-

https://doi.org/10.1007/s10118-023-2958-7

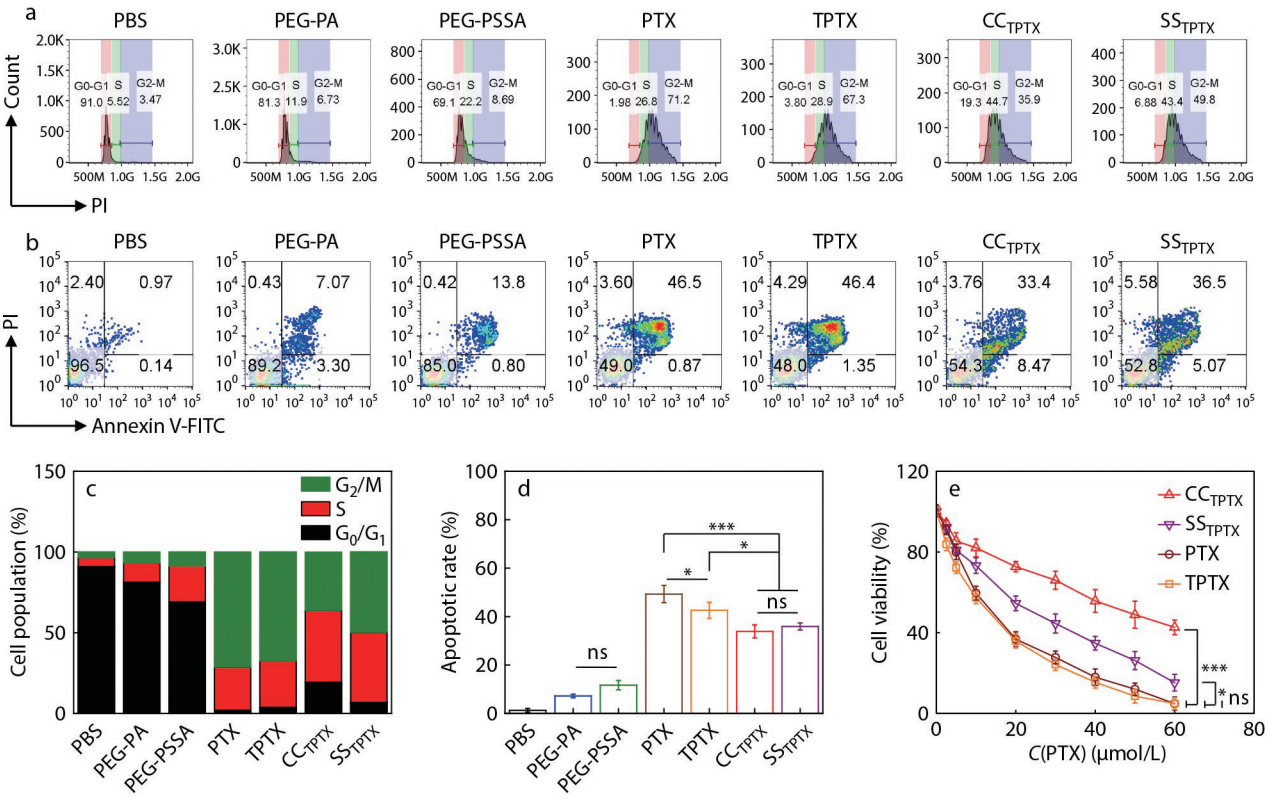

Fig. 5 (a) Cell cycle analyses of 4T1 cells after 24 h incubation with various drugs; (b) Apoptosis assay of 4T1 cells after 24 h incubation with various drugs; (c, d) Quantitative assays of cell cycle (c) and apoptosis (d); (e) Cell viability of 4T1 cells following 24 h incubation with PTX, TPTX, CC_{TPTX}, and SS_{TPTX}. Data are presented as mean±SD (n=3, $^{**}p$<0.01, $^{***}p$<0.001).

ured with MTT assay (Fig. 5e). The results show that both PEG-PA and PEG-PSSA were almost non-toxic to cells (Fig. S5 in ESI). Consistent with the cell cycle arrest and apoptosis assay, TPTX showed similar cytotoxicity as PTX, with IC50 of 13.65 and 16.10 μmol/L being observed, respectively. For the drug-loaded nanoparticles, the IC50 values of CC_{TPTX} (47.55 μmol/L) was significantly higher than SS_{TPTX} (20.76 μmol/L), further corroborating the advantage of the GSH-sensitivity of the vehicle.

Biodistribution and CT Imaging of Prodrug Nanoparticles

Given that as-prepared prodrug nanoparticles have exhibited excellent *in vitro* stability and tumor cell-killing effect, we further studied the *in vivo* tumor targeting ability. A subcutaneous 4T1 tumor model was established by injecting 100 μL of serum-free medium containing 3.0×10^6 4T1 cells. Free Cy7.5 and Cy7.5-loaded nanoparticles were injected through the tail vein to investigate the biodistribution. Compared with free Cy7.5 which was rapidly eliminated from the body and rarely enriched in the tumor site, SS_{TPTX} shows obvious tumor accumulation from 1 h to 24 h after injection (Fig. 6a), indicating the nanoparticles accumulation and retention at the tumor site. There are two possible reasons for the significantly weaker fluorescence of CC_{TPTX} at tumor site. One is the smaller size of CC_{TPTX} nanoparticles which might led to rapider elimination and weaker tumor accumulation.[49] The other is the aggregation-induced fluorescence quenching of Cy7.5 molecules inside nanoparticles which could be weaken due to the GSH-responsive disassembly of SS_{TPTX} nanoparticles.[50] After the injection of nanoparticles for 24 h, the *ex vivo* imaging and the quantitative analysis (Fig. 6b) of the fluorescence intensity in various organs further demonstrated the tumor-targeting ability of the prodrug nanoparticles.

CT imaging can help the early diagnosis of tumor occurrence and metastasis.[51] To evaluate the CT contrast enhancing capacity of as-prepared iodinated nanoparticles, commercially available Iohexol was used in the experiments. As shown in Figs. 6(c) and 6(d), similar concentration-dependent contrast enhancement could be observed for free Iohexol, CC_{TPTX} and SS_{TPTX}. The *in vivo* contrast enhancement data after *i.v.* injection of PEG-PSSA could further corroborate these findings (Figs. 6e and 6f). According to the CT values of the heart region at 0 h after injection (Fig. 6f), as-prepared nanoparticles show excellent contrast enhancing ability, with ΔHu of 120 being observed. Notably, similar ΔHu could be observed at 0 and 1 h after injection, suggesting that as-prepared nanoparticles could enhance the CT contrast in relatively long period which allowed the acquisition of more detailed information. Moreover, this also provided an important strategy for potential CT image-guided cancer treatment.

In vivo Anti-Tumor Effect of Prodrug Nanoparticles

The *in vivo* antitumor efficacy of various drugs was evaluated in a subcutaneous 4T1 model. Mice received *i.v.* injection of 5 mg/kg of PBS, PTX, TPTX, CC_{TPTX} or SS_{TPTX} at every 2 days for a total of four times. Tumor volume (Fig. 7a) and body weight change (Fig. 7c) were recorded at every 2 days. At the end of the

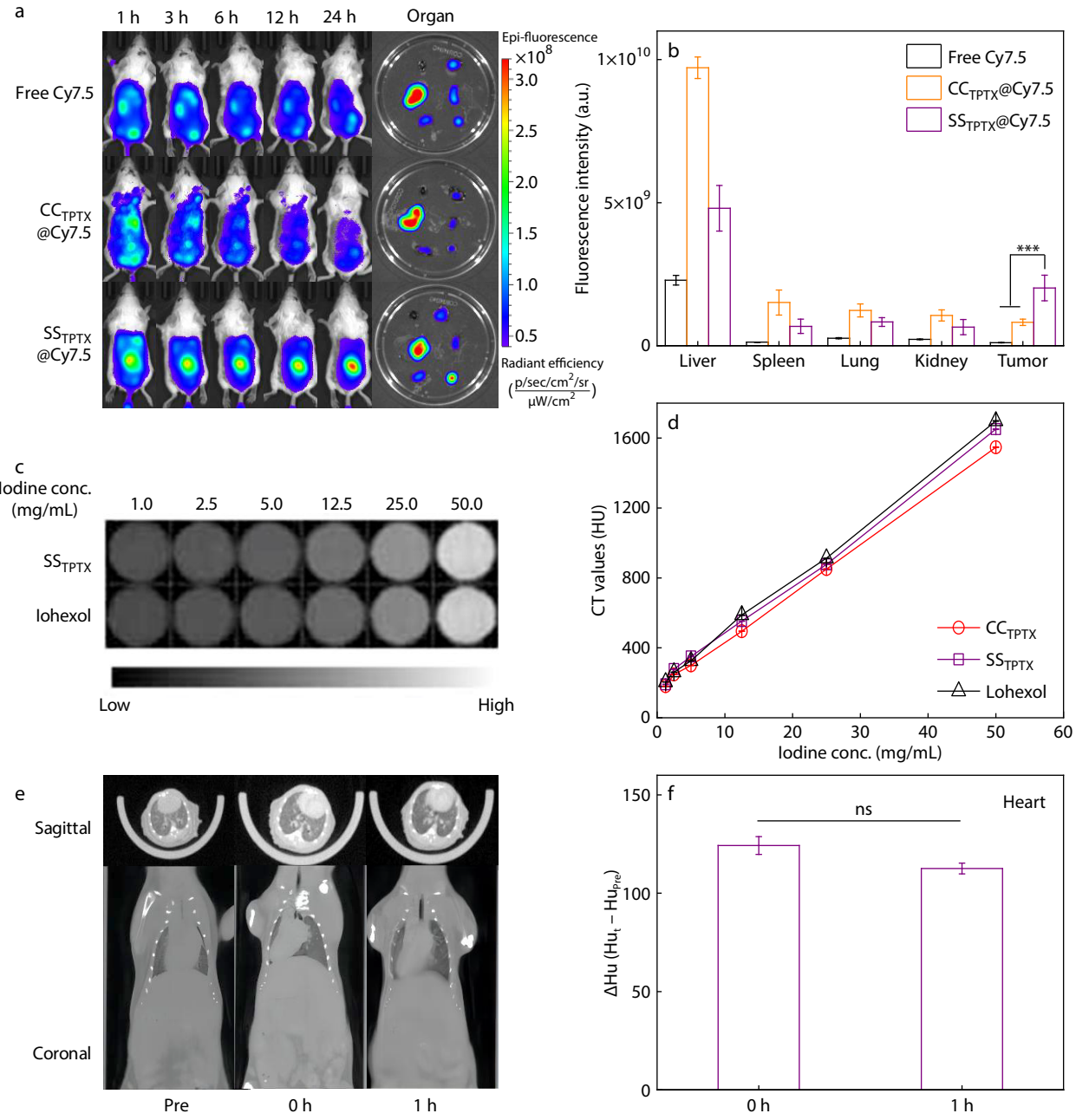

Fig. 6 (a) Fluorescence images of orthotopic 4T1 tumor-bearing mice at different time points following injection of free Cy7.5 or Cy7.5 labeled prodrug nanoparticles; (b) Quantification of drug accumulation in different organs at 24 h after injection of free Cy7.5 or Cy7.5 labeled prodrug nanoparticles; (c, d) CT images and CT values of different concentrations of polymer nanoparticles and Iohexol *in vitro*; (e) CT Imaging of polymer nanoparticles in mice; (f) Quantification of the CT enhancement values at the heart region of mice. Data are presented as mean±SD (n=3, $^{**}p$<0.01, $^{***}p$<0.001).

treatment, the mice were sacrificed under anesthesia; then the tumors and major organs were excised. As shown in Figs. 7(a) and 7(b), in the PBS group, the tumor volume reaches 25.95 times of the initial value. Compared to PBS group, the tumor volume at 16 days after treatments with PTX, TPTX, CC$_{TPTX}$ and SS$_{TPTX}$ reaches 3.78, 10.23, 9.0 and 3.13 times of the initial value, respectively. Even though free PTX significantly inhibited the tumor growth, it also caused significant body weight loss. Despite that TPTX exhibited similar *in vitro* cancer cell killing effects as PTX, less significant tumor growth inhibition was achieved, possibly due to the more hydrophobic nature of TPTX. The less body weight loss for TPTX compared with PTX further proved the advantages of prodrug strategy in terms of safety. Moreover, it should be noted that SS$_{TPTX}$ showed the most significant tumor growth inhibition effect, with no obvious body weight being observed at the same time.

At the end of the experiments, the excised tumors were subjected to H&E, TUNEL, and Ki67 staining (Fig. 7d). Meanwhile, H&E staining was also carried out for the normal organ slices (Fig. S6 in ESI). As shown in Fig. 7(d), among various

https://doi.org/10.1007/s10118-023-2958-7

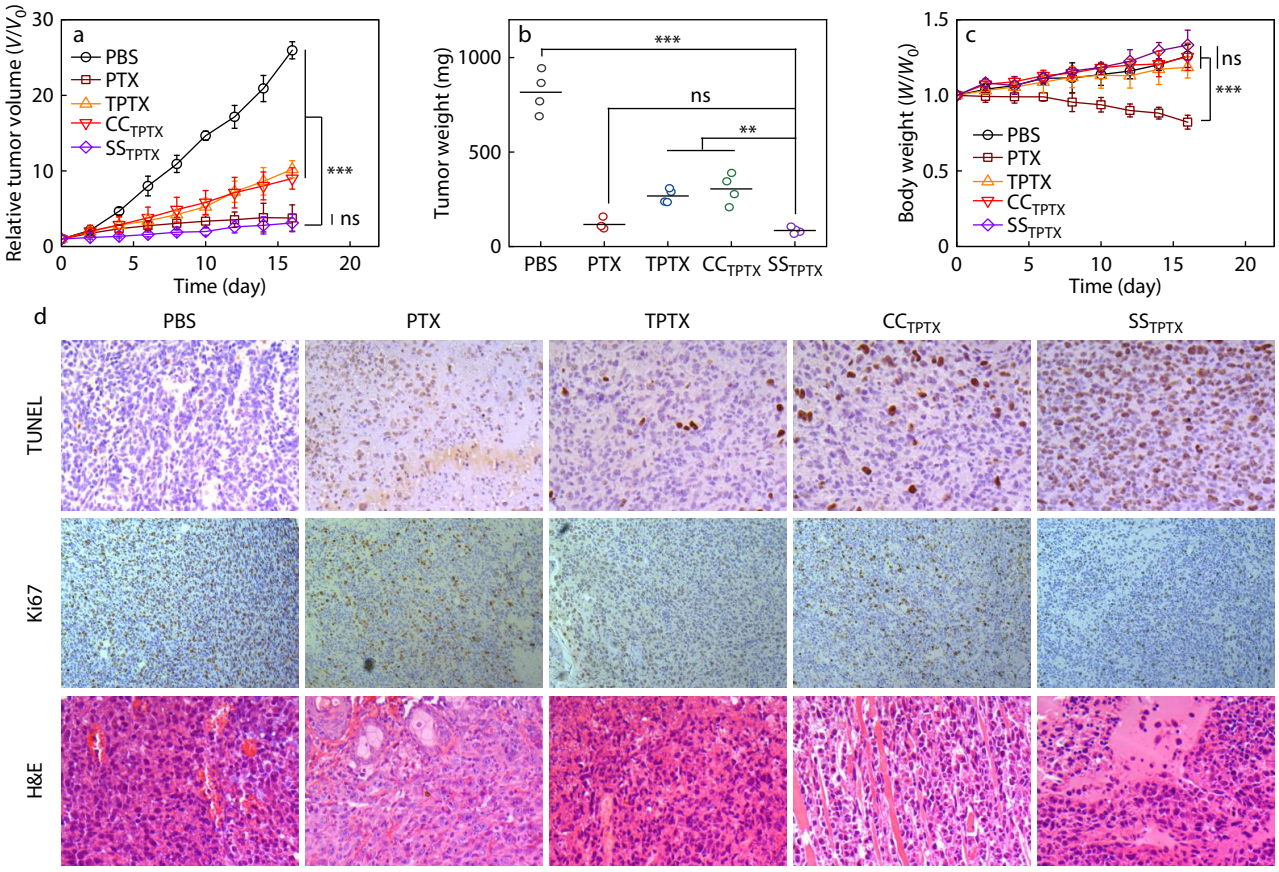

Fig. 7 (a) Relative tumor volume changes of various groups after different treatments; (b) Tumor weight of various groups after different treatments; (c) Body weight changes of mice in various groups after different treatments; (d) TUNEL, Ki-67 and H&E staining images of tumor tissues collected from mice treated with various drugs. Scale bars=100 μm. Data are presented as mean±SD (n=4, $^{**}p$<0.01, $^{***}p$<0.001).

treatments, PTX and SS_{TPTX} led to the most apoptotic cells and the least proliferated cells in tumor tissues. The massive necrotic region in the PTX and SS_{TPTX} groups could further reveal their excellent anticancer efficacy. The steady body weight and the normal H&E staining results of major organs (heat, lung, liver, spleen and kidney) collected from SS_{TPTX} treated mice further suggested its safety profiles. The results showed that the prodrug nanoparticles owned certain selectivity between cancer cells and normal cells. In addition to differences in GSH, prodrugs after esterification of PTX may be more easily activated in cancer cells.[52] Collectively, the above data indicated that as-prepared GSH-sensitive prodrug nanoparticles could not only inhibit tumor growth but also avoid the toxic effect of PTX.

CONCLUSIONS

In summary, to achieve the safe imaging-guided tumor therapy, we have developed a iodinated GSH-responsive prodrug nanomedicine. With the benefit of the prodrug strategy, efficient drug loading capacity and cancer cell selectivity could be achieved. The GSH-sensitivity facilitated the inracellular drug delivery so that the prodrug nanoparticles could efficiently kill cancer cells. The *in vivo* biodistribution and imaging studies have revealed that the stable nanoparticles could selectively accumulate in tumor tissue and significantly enhance CT contrast in the blood pool. Moreover, due to passive targeting effect and redox-responsive drug delivery, as-prepared nanoparticles could promptly deliver drugs to tumor cells to exert highly potent anticancer efficacy. Importantly, unlike the free PTX which caused significant body weight loss, as-prepared prodrug nanoparticles did not show significant toxicity. Collectively, the advantages of as-designed iodinated redox-responsive nanomedicine made it a potential candidate for imaging-guided anticancer therapy, with which tumor inhibition and therapeutic efficacy evaluation were expected to be achieved at the same time.

Conflict of Interests

The authors declare no interest conflict.

Electronic Supplementary Information

Electronic supplementary information (ESI) is available free of charge in the online version of this article at http://doi.org/10.1007/s10118-023-2958-7.

ACKNOWLEDGMENTS

This work was financially supported by the National Natural Science Foundation of China (Nos. 51973014, 52033001 and

21774008) and the long-term subsidy mechanism from the Ministry of Finance and the Ministry of Education of PRC for BUCT and the Fundamental Research Funds for the Central Universities of China (Nos. BUCTRC201912, XK1701 and XK1802-8).

REFERENCES

1 Lammers, T.; Aime, S.; Hennink, W. E.; Storm, G.; Kiessling, F. Theranostic nanomedicine. *Acc. Chem. Res.* **2011**, *44*, 1029–1038.
2 Ma, X.; Zhao, Y.; Liang, X. J. Theranostic nanoparticles engineered for clinic and pharmaceutics. *Acc. Chem. Res.* **2011**, *44*, 1114–1122.
3 Ryu, J. H.; Koo, H.; Sun, I. C.; Yuk, S. H.; Choi, K.; Kim, K.; Kwon, I. C. Tumor-targeting multi-functional nanoparticles for theragnosis: new paradigm for cancer therapy. *Adv. Drug Deliv. Rev.* **2012**, *64*, 1447–1458.
4 Lee, D. E.; Koo, H.; Sun, I. C.; Ryu, J. H.; Kim, K.; Kwon, I. C. Multifunctional nanoparticles for multimodal imaging and theragnosis. *Chem. Soc. Rev.* **2012**, *41*, 2656–72.
5 Al-Buriahi, M. S.; Tonguc, B. T. Mass attenuation coefficients, effective atomic numbers and electron densities of some contrast agents for computed tomography. *Radiat. Phys. Chem.* **2020**, *166*, 108507.
6 Wang, M.; Chang, M.; Chen, Q.; Wang, D.; Li, C.; Hou, Z.; Lin, J.; Jin, D.; Xing, B. Au(2)Pt-PEG-Ce6 nanoformulation with dual nanozyme activities for synergistic chemodynamic therapy/phototherapy. *Biomaterials* **2020**, *252*, 120093.
7 Choi, J. Y.; Lee, J. M.; Sirlin, C. B. CT and MR imaging diagnosis and staging of hepatocellular carcinoma: Part II. Extracellular agents, hepatobiliary agents, and ancillary imaging features. *Radiology* **2014**, *273*, 30–50.
8 Liu, Y.; Ai, K.; Lu, L. Nanoparticulate X-ray computed tomography contrast agents: from design validation to *in vivo* applications. *Acc. Chem. Res.* **2012**, *45*, 1817–1827.
9 Lee, N.; Choi, S. H.; Hyeon, T. Nano-sized CT contrast agents. *Adv. Mater.* **2013**, *25*, 2641–2660.
10 Potier, M.; Lagroye, I.; Lakhdar, B.; Cambar, J.; Idee, J. M. Comparative cytotoxicity of low- and high-osmolar contrast media to human fibroblasts and rat mesangial cells in culture. *Invest. Radiol.* **1997**, *32*, 621–626.
11 Hallouard, F.; Anton, N.; Choquet, P.; Constantinesco, A.; Vandamme, T. Iodinated blood pool contrast media for preclinical X-ray imaging applications—a review. *Biomaterials* **2010**, *31*, 6249–6268.
12 Zhang, W. L.; Li, N.; Huang, J.; Yu, J. H.; Wang, D. X.; Li, Y. P.; Liu, S. Y. Gadolinium-conjugated FA-PEG-PAMAM-COOH nanoparticles as potential tumor-targeted circulation-prolonged macromolecular MRI contrast agents. *J. Appl. Polym. Sci.* **2010**, *118*, 1805–1814.
13 Yan, J.; Yin, M.; Foster, F. S.; Démoré, C. E. M. Tumor contrast imaging with gas vesicles by circumventing the reticulo-endothelial system. *Ultrasound Med. Biol* **2020**, *46*, 359–368.
14 Rajendran, K.; Petersilka, M.; Henning, A.; Shanblatt, E. R.; Schmidt, B.; Flohr, T. G.; Ferrero, A.; Baffour, F.; Diehn, F. E.; Yu, L.; Rajiah, P.; Fletcher, J. G.; Leng, S.; McCollough, C. H. First clinical photon-counting detector CT system: technical evaluation. *Radiology* **2021**, *303*, 130–138.
15 Bhatt, S. P.; Soler, X.; Wang, X.; Murray, S.; Anzueto, A. R.; Beaty, T. H.; Boriek, A. M.; Casaburi, R.; Criner, G. J.; Diaz, A. A.; Dransfield, M. T.; Curran-Everett, D.; Galban, C. J.; Hoffman, E. A.; Hogg, J. C.; Kazerooni, E. A.; Kim, V.; Kinney, G. L.; Lagstein, A.; Lynch, D. A.; Make, B. J.; Martinez, F. J.; Ramsdell, J. W.; Reddy, R.; Ross, B. D.; Rossiter, H. B.; Steiner, R. M.; Strand, M. J.; van Beek, E. J.; Wan, E. S.; Washko, G. R.; Wells, J. M.; Wendt, C. H.; Wise, R. A.; Silverman, E. K.; Crapo, J. D.; Bowler, R. P.; Han, M. K.; Investigators, C. O. Association between functional small airway disease and FEV1 decline in chronic obstructive pulmonary disease. *Am. J. Respir. Crit. Care Med.* **2016**, *194*, 178–84.
16 Smit, J.; Borm, F. J.; Niemeijer, A. N.; Huisman, M. C.; Hoekstra, O. S.; Boellaard, R.; Oprea-Lager, D. E.; Vugts, D. J.; van Dongen, G.; de Wit-van der Veen, B. J.; Thunnissen, E.; Smit, E. F.; de Langen, A. J. PD-L1 PET/CT imaging with radiolabeled durvalumab in patients with advanced-stage non-small cell lung cancer. *J. Nucl. Med.* **2022**, *63*, 686–693.
17 Sartor, O.; de Bono, J.; Chi, K. N.; Fizazi, K.; Herrmann, K.; Rahbar, K.; Tagawa, S. T.; Nordquist, L. T.; Vaishampayan, N.; El-Haddad, G.; Park, C. H.; Beer, T. M.; Armour, A.; Perez-Contreras, W. J.; DeSilvio, M.; Kpamegan, E.; Gericke, G.; Messmann, R. A.; Morris, M. J.; Krause, B. J.; Investigators, V. Lutetium-177-PSMA-617 for metastatic castration-resistant prostate cancer. *N. Engl. J. Med.* **2021**, *385*, 1091–1103.
18 Liu, Q.; Qian, Y.; Li, P.; Zhang, S.; Liu, J.; Sun, X.; Fulham, M.; Feng, D.; Huang, G.; Lu, W.; Song, S. ^{131}I-labeled copper sulfide-loaded microspheres to treat hepatic tumors *via* hepatic artery embolization. *Theranostics* **2018**, *8*, 785–799.
19 Zhu, J.; Wang, G.; Alves, C. S.; Tomás, H.; Xiong, Z.; Shen, M.; Rodrigues, J.; Shi, X. Multifunctional dendrimer-entrapped gold nanoparticles conjugated with doxorubicin for pH-responsive drug delivery and targeted computed tomography imaging. *Langmuir* **2018**, *34*, 12428–12435.
20 Zalcman, G.; Mazieres, J.; Margery, J.; Greillier, L.; Audigier-Valette, C.; Moro-Sibilot, D.; Molinier, O.; Corre, R.; Monnet, I.; Gounant, V.; Rivière, F.; Janicot, H.; Gervais, R.; Locher, C.; Milleron, B.; Tran, Q.; Lebitasy, M. P.; Morin, F.; Creveuil, C.; Parienti, J. J.; Scherpereel, A. Bevacizumab for newly diagnosed pleural mesothelioma in the Mesothelioma Avastin Cisplatin Pemetrexed Study (MAPS): a randomised, controlled, open-label, phase 3 trial. *Lancet* **2016**, *387*, 1405–1414.
21 Danhier, F.; Lecouturier, N.; Vroman, B.; Jerome, C.; Marchand-Brynaert, J.; Feron, O.; Preat, V. Paclitaxel-loaded PEGylated PLGA-based nanoparticles: *in vitro* and *in vivo* evaluation. *J. Control. Rel.* **2009**, *133*, 11–17.
22 Zhao, J.; Du, J.; Wang, J.; An, N.; Zhou, K.; Hu, X.; Dong, Z.; Liu, Y. Folic acid and poly(ethylene glycol) decorated paclitaxel nanocrystals exhibit enhanced stability and breast cancer-targeting capability. *ACS Appl. Mater. Interfaces* **2021**, *13*, 14577–14586.
23 Liu, Y.; Guo, K.; Ding, M.; Zhang, B.; Xiao, N.; Tang, Z.; Wang, Z.; Zhang, C.; Shubhra, Q. T. H. Engineered magnetic polymer nanoparticles can ameliorate breast cancer treatment inducing pyroptosis-starvation along with chemotherapy. *ACS Appl. Mater. Interfaces* **2022**, *14*, 42541–42557.
24 Das, T.; Nandy, S.; Pandey, D. K.; Al-Tawaha, A. R.; Swamy, M. K.; Kumar, V.; Nongdam, P.; Dey, A. 12-An update on paclitaxel treatment in breast cancer. *Paclitaxel* **2022**, 287–308.
25 Li, L.; Zhan, Q.; Yi, K.; Chen, N.; Li, X.; Yang, S.; Hou, X.; Zhao, J.; Yuan, X.; Kang, C. Engineering Lipusu with lysophosphatidylcholine for improved tumor cellular uptake and anticancer efficacy. *J. Mater. Chem. B* **2022**, *10*, 1833–1842.
26 Chen, Q.; Xu, S.; Liu, S.; Wang, Y.; Liu, G. Emerging nanomedicines of paclitaxel for cancer treatment. *J. Control. Rel.* **2022**, *342*, 280–294.
27 Luo, C.; Sun, J.; Liu, D.; Sun, B.; Miao, L.; Musetti, S.; Li, J.; Han, X.; Du, Y.; Li, L.; Huang, L.; He, Z. Self-assembled redox dual-responsive prodrug-nanosystem formed by single thioether-bridged paclitaxel-fatty acid conjugate for cancer chemotherapy. *Nano Lett.* **2016**, *16*, 5401–5408.
28 Pei, Q.; Hu, X.; Zheng, X.; Liu, S.; Li, Y.; Jing, X.; Xie, Z. Light-

activatable red blood cell membrane-camouflaged dimeric prodrug nanoparticles for synergistic photodynamic/chemotherapy. *ACS Nano* **2018**, *12*, 1630–1641.
29 Luo, T.; Loira-Pastoriza, C.; Patil, H. P.; Ucakar, B.; Muccioli, G. G.; Bosquillon, C.; Vanbever, R. PEGylation of paclitaxel largely improves its safety and anti-tumor efficacy following pulmonary delivery in a mouse model of lung carcinoma. *J. Control. Rel.* **2016**, *239*, 62–71.
30 Yang, D.; Liu, X.; Jiang, X.; Liu, Y.; Ying, W.; Wang, H.; Bai, H.; Taylor, W. D.; Wang, Y.; Clamme, J. P.; Co, E.; Chivukula, P.; Tsang, K. Y.; Jin, Y.; Yu, L. Effect of molecular weight of PGG–paclitaxel conjugates on *in vitro* and *in vivo* efficacy. *J. Control. Rel.* **2012**, *161*, 124–131.
31 Jiang, M.; Zhang, R.; Wang, Y.; Jing, W.; Liu, Y.; Ma, Y.; Sun, B.; Wang, M.; Chen, P.; Liu, H.; He, Z. Reduction-sensitive paclitaxel prodrug self-assembled nanoparticles with tetrandrine effectively promote synergistic therapy against drug-sensitive and multidrug-resistant breast cancer. *Mol. Pharmaceutics* **2017**, *14*, 3628–3635.
32 Zhai, Y.; Zhou, X.; Jia, L.; Ma, C.; Song, R.; Deng, Y.; Hu, X.; Sun, W. Acetal-linked paclitaxel polymeric prodrug based on functionalized mPEG-PCL diblock polymer for pH-triggered drug delivery. *Polymers* **2017**, *9*, 698.
33 Zhang, X.; He, F.; Xiang, K.; Zhang, J.; Xu, M.; Long, P.; Su, H.; Gan, Z.; Yu, Q. CD44-targeted facile enzymatic activatable chitosan nanoparticles for efficient antitumor therapy and reversal of multidrug resistance. *Biomacromolecules* **2018**, *19*, 883–895.
34 Yi, X.; Hu, J. J.; Dai, J.; Lou, X.; Zhao, Z.; Xia, F.; Tang, B. Z. Self-guiding polymeric prodrug micelles with two aggregation-induced emission photosensitizers for enhanced chemo-photodynamic therapy. *ACS Nano* **2021**, *15*, 3026–3037.
35 Li, Y.; Jiang, Y.; Zheng, Z.; Du, N.; Guan, S.; Guo, W.; Tang, X.; Cui, J.; Zhang, L.; Liu, K.; Yu, Q.; Gan, Z. Co-delivery of precisely prescribed multi-prodrug combination by an engineered nanocarrier enables efficient individualized cancer chemotherapy. *Adv. Mater.* **2022**, *34*, e2110490.
36 Wang, Z.; Yang, C.; Zhang, H.; Gao, Y.; Xiao, M.; Wang, Z.; Yang, L.; Zhang, J.; Ren, C.; Liu, J. *In situ* transformable supramolecular nanomedicine targeted activating hippo pathway for triple-negative breast cancer growth and metastasis inhibition. *ACS Nano* **2022**, *16*, 14644–14657.
37 Zhang, C.; Meng, X.; Gong, C.; Zhao, J.; Zhang, K.; Yang, Z. Glutathione-responsive biodegradable nanoplatform with endogenous esterase-triggered nitric oxide release for gas therapy and enhanced chemotherapy. *ACS Appl. Bio Mater.* **2021**, *4*, 5212–5221.
38 Yu, K.; Hai, X.; Yue, S.; Song, W.; Bi, S. Glutathione-activated DNA-Au nanomachine as targeted drug delivery platform for imaging-guided combinational cancer therapy. *Chem. Eng. J.* **2021**, *419*, 129535.
39 Tan, P.; Cai, H.; Wei, Q.; Tang, X.; Zhang, Q.; Kopytynski, M.; Yang, J.; Yi, Y.; Zhang, H.; Gong, Q.; Gu, Z.; Chen, R.; Luo, K. Enhanced chemo-photodynamic therapy of an enzyme-responsive prodrug in bladder cancer patient-derived xenograft models. *Biomaterials* **2021**, *277*, 121061.
40 Corrigan, N.; Jung, K.; Moad, G.; Hawker, C. J.; Matyjaszewski, K.; Boyer, C. Reversible-deactivation radical polymerization (controlled/living radical polymerization): from discovery to materials design and applications. *Prog. Polym. Sci.* **2020**, *111*, 101311.
41 Quan, H.; Fan, L.; Huang, Y.; Xia, X.; He, Y.; Liu, S.; Yu, J. Hyaluronic acid-decorated carborane-TAT conjugation nanomicelles: a potential boron agent with enhanced selectivity of tumor cellular uptake. *Colloids Surf. B* **2021**, *204*, 111826.
42 Cheng, R.; Feng, F.; Meng, F.; Deng, C.; Feijen, J.; Zhong, Z. Glutathione-responsive nano-vehicles as a promising platform for targeted intracellular drug and gene delivery. *J. Control. Rel.* **2011**, *152*, 2–12.
43 Cuggino, J. C.; Gatti, G.; Picchio, M. L.; Maccioni, M.; Gugliotta, L. M.; Alvarez Igarzabal, C. I. Dually responsive nanogels as smart carriers for improving the therapeutic index of doxorubicin for breast cancer. *Eur. Polym. J.* **2019**, *116*, 445–452.
44 Jin, Q.; Deng, Y.; Chen, X.; Ji, J. Rational design of cancer nanomedicine for simultaneous stealth surface and enhanced cellular uptake. *ACS Nano* **2019**, *13*, 954–977.
45 Khorsand, B.; Lapointe, G.; Brett, C.; Oh, J. K. Intracellular drug delivery nanocarriers of glutathione-responsive degradable block copolymers having pendant disulfide linkages. *Biomacromolecules* **2013**, *14*, 2103–2111.
46 Borkowska, M.; Siek, M.; Kolygina, D. V.; Sobolev, Y. I.; Lach, S.; Kumar, S.; Cho, Y. K.; Kandere-Grzybowska, K.; Grzybowski, B. A. Targeted crystallization of mixed-charge nanoparticles in lysosomes induces selective death of cancer cells. *Nat. Nanotechnol.* **2020**, *15*, 331–341.
47 Qian, J.; Xu, Z.; Meng, C.; Liu, Y.; Wu, H.; Wang, Y.; Yang, J.; Zheng, H.; Ran, F.; Liu, G. Q.; Ling, Y. Redox-activatable theranostic co-prodrug for precise tumor diagnosis and selective combination chemotherapy. *J. Med. Chem.* **2022**, *65*, 10393–10407.
48 Angelucci, A.; Mari, M.; Millimaggi, D.; Giusti, I.; Carta, G.; Bologna, M.; Dolo, V. Suberoylanilide hydroxamic acid partly reverses resistance to paclitaxel in human ovarian cancer cell lines. *Gynecol. Oncol.* **2010**, *119*, 557–563.
49 Cheng, G.; Zong, W.; Guo, H.; Li, F.; Zhang, X.; Yu, P.; Ren, F.; Zhang, X.; Shi, X.; Gao, F.; Chang, J.; Wang, S. Programmed size-changeable nanotheranostic agents for enhanced imaging-guided chemo/photodynamic combination therapy and fast elimination. *Adv. Mater.* **2021**, *33*, 2100398.
50 Kelkar, S. S.; Hill, T. K.; Marini, F. C.; Mohs, A. M. Near infrared fluorescent nanoparticles based on hyaluronic acid: self-assembly, optical properties, and cell interaction. *Acta Biomater.* **2016**, *36*, 112–121.
51 Ginn-Hedman, A. M.; Self, T. S.; Jessen, S. L.; Heaps, C. L.; Weeks, B. R.; Clubb, F. J. Jr. Diffusible contrast-enhanced micro-CT improves visualization of stented vessels. *Cardiovasc. Pathol.* **2022**, *60*, 107428.
52 Louage, B.; Van Steenbergen, M. J.; Nuhn, L.; Risseeuw, M. D. P.; Karalic, I.; Winne, J.; Van Calenbergh, S.; Hennink, W. E.; De Geest, B. G. Micellar paclitaxel-initiated RAFT polymer conjugates with acid-sensitive behavior. *ACS Macro Lett.* **2017**, *6*, 272–276.

https://doi.org/10.1007/s10118-023-2958-7